

Coupling Of The B_{1g} Phonon To The Anti-Nodal Electronic States of $\text{Bi}_2\text{Sr}_2\text{Ca}_{0.92}\text{Y}_{0.08}\text{Cu}_2\text{O}_{8+\delta}$

T. Cuk,¹ F. Baumberger,¹ D.H. Lu,¹ N. Ingle,¹ X.J. Zhou,¹ H. Eisaki,^{2,1}
N. Kaneko,¹ Z. Hussain,³ T.P. Devereaux,⁴ N. Nagaosa,⁵ and Z.-X. Shen^{1,6}

¹*Departments of Physics, Applied Physics and Stanford Synchrotron
Radiation Laboratory, Stanford University, Stanford, CA 94305*

²*Nanoelectronics Research Institute, National Institute of Advanced Industrial Science and Technology,
1-1-1 Central 2, Umezono, Tsukuba, Ibaraki, 305-8568, Japan*

³*Advanced Light Source, Lawrence Berkeley National Laboratory, Berkeley, California 94720, USA*

⁴*Dept. of Physics University of Waterloo Waterloo, ON CANADA, N2L 3G1*

⁵*CREST, Department of Applied Physics, University of Tokyo, Bunkyo-ku, Tokyo 113, Japan*

⁶*Physics Institute, University of Zurich, Zurich, CH-8057, Switzerland*

(Dated: October 5, 2003)

Angle-resolved photoemission spectroscopy (ARPES) on optimally doped $\text{Bi}_2\text{Sr}_2\text{Ca}_{0.92}\text{Y}_{0.08}\text{Cu}_2\text{O}_{8+\delta}$ uncovers a coupling of the electronic bands to a 40 meV mode in an extended k-space region away from the nodal direction, leading to a new interpretation of the strong renormalization of the electronic structure seen in $\text{Bi}2212$. Phenomenological agreements with neutron and Raman experiments suggest that this mode is the B_{1g} oxygen bond-buckling phonon. A theoretical calculation based on this assignment reproduces the electronic renormalization seen in the data.

The discovery of bosonic renormalization effects in cuprate superconductors in the form of a dispersion “kink” near 50-70 meV for the nodal state has attracted considerable interest [1, 2, 3, 4, 5]. While a consensus has been reached that the renormalization is due to electronic coupling to a bosonic mode, disagreement remains as to whether the assignment to a phononic or an electronic mode is more appropriate. More recently, another “kink” phenomenon has been reported for the antinodal electronic state near $(\pi, 0)$ [5, 6, 7, 8]. In contrast to the nodal renormalization, which shows little change across T_c , the antinodal renormalization has been observed so far only below T_c . The strong temperature dependence and the dominance of the coupling strength near $(\pi, 0)$ have been taken as evidence to identify the bosonic mode with the 41meV spin resonance [5, 6, 7, 8].

At first glance, the spin mode appears to provide a natural interpretation for the antinodal kink. The spin mode turns on at T_c and has a well-defined momentum of (π, π) which preentially connects the anti-nodal states. However, serious issues remain. The prominent kink in ARPES is observed in deeply overdoped samples where no evidence of a spin resonance exists [6, 7]. Further, there is a serious debate as to whether the spin resonance has sufficient spectral weight to cause the observed bosonic renormalization effect [9, 10, 11].

In this letter, we present extensive temperature, momentum, and doping dependent ARPES data from $\text{Bi}_2\text{Sr}_2\text{Ca}_{0.92}\text{Y}_{0.08}\text{Cu}_2\text{O}_{8+\delta}$ that demonstrate the persistence of a dispersion break near 40meV in the normal state close to $(\pi, 0)$, invalidating the spin resonance interpretation. In the superconducting state, the energy scale of this mode shifts to ~ 65 -70meV and the signatures of coupling increase considerably. We show that the

~ 40 meV B_{1g} oxygen “bond-buckling” phonon has the correct energy and coupling anisotropy from its $d_{x^2-y^2}$ symmetry [12, 13] that, in conjunction with the underlying band-structure anisotropy, naturally explains the momentum dependence of the $(\pi, 0)$ kink. We attribute the temperature dependence to the density of states enhancement due to the superconducting gap opening and to the thermal broadening of the phonon self energy in the normal state. Calculations using an electron-phonon coupling vertex of B_{1g} symmetry reproduce the experimental data.

ARPES experiments have been preformed at beamline V-4 of the Stanford Synchrotron Radiation Laboratory with a photon energy of 22.7eV. The energy and angular resolutions are 14 meV and ± 0.15 degree, respectively. Optimally doped $\text{Bi}_2\text{Sr}_2\text{Ca}_{0.92}\text{Y}_{0.08}\text{Cu}_2\text{O}_{8+\delta}$ ($T_c = 94\text{K}$) samples were cleaved in situ with a base pressure of 4×10^{-11} torr. Key data have been reproduced in two other experimental chambers.

In Fig. 1, data in the anti-nodal region reveal a dramatic change in the effective coupling through T_c . In the superconducting state, classical Engelsberg-Schrieffer signatures of electronic coupling to a bosonic mode are seen in the Energy Distribution Curves (EDCs) (Fig. 1b1) and the image plot (Fig. 1b2): 1) a break up into two branches—a peak that decays as it asymptotically approaches a characteristic energy at 70meV, and a hump that traces out a roughly parabolic band. The peak that asymptotically approaches the mode energy derives from strong mixing of the electronic band with the mode, while the hump traces out the bare band dispersion away from the mode energy (the peaks are indicated by “I” and the humps by “II” in Fig. 1b1; the peaks correspond to the trail of intensity above the indicated point in Fig. 1b2);

2) a significant broadening of the spectra beyond 70meV due to the onset of the bosonic mode self energy[14].

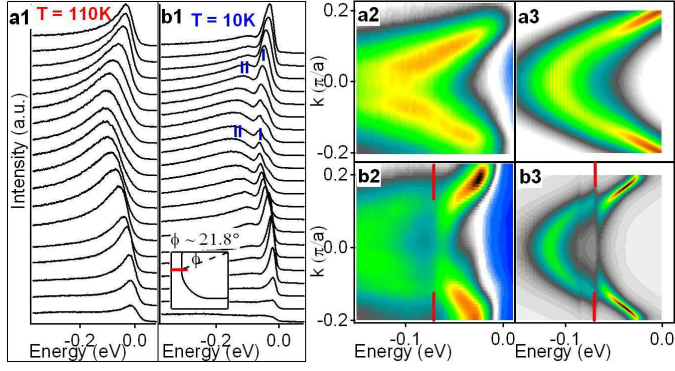


FIG. 1: a1) and b1) EDCs taken at 110K and 15K, respectively, at the k-space location indicated in the inset of b1). The corresponding image plots are shown in a2) and b2). Image plots of the calculations are shown in a3) and b3) at 110K and 15K respectively. Color scales are independent for each image plot.

In the normal state (Fig. 1a1, 1a2) little of these effects can be seen without further analysis. In Fig. 2, we have extracted dispersions for three k-space cuts in a momentum space region between the nodal direction and the Van Hove Singularity (VHS) at $(\pi, 0)$. Since we are only concerned with the energy scale, we fit the Energy Distribution Curves (EDCs) phenomenologically. The usual method to extract dispersions—fitting Momentum Distribution Curves with Lorentzians—is not appropriate since the assumed linear approximation of the bare band fails towards $(\pi, 0)$ where the band bottom is close to E_F [15]. EDC-derived dispersions of three independent data sets shown in Fig. 2 (a1,b1,c) consistently reveal a $\sim 40\text{meV}$ energy scale that has eluded detection before [5, 6, 7, 8].

One may be concerned about a distortion to the dispersion due to bilayer splitting. However, the 40 meV mode has been clearly observed in two other cases that are independent of bilayer effects—in deeply over-doped samples below T_c where the gap is small, for which the bilayer splitting is well-resolved [7], and in normal state optics data near optimal doping for which spectra are averaged over the Brillouin Zone, thereby washing out any sharp structure due to the dispersion of bilayer splitting [16]. Further, while the bilayer splitting is different under the three circumstances shown in Fig. 2 (a1, b1, c), the kink energy remains the same. Finally, while certain peak-dip-hump features have been attributed to bilayer splitting when well-resolved, “kink” features in the dispersions cannot be accounted for in this way (two nearly parallel bands alone do not reproduce the effect).

In Fig. 2, we also show the temperature dependence of this 40meV kink through a comparison of the dispersions. In the superconducting state, the EDC peak posi-

tion asymptotically approaches the characteristic energy defined by the bosonic mode (Fig. 2a2, Fig. 2b2). Because the effect is much stronger below T_c , it is clearly revealed in the MDC dispersion also; the kink position indicates the characteristic energy and the kink sharpness monotonically increases with the coupling strength. In addition to the increase in effective coupling strength, the data show that the kink energy shifts from $\sim 40\text{meV}$ to $\sim 65\text{--}70\text{meV}$. This is an important observation since the opening of a superconducting gap is expected to shift the energy at which the electronic states couple to the bosonic mode and has thus far not been detected by ARPES. Here, we observe a kink shift of $\sim 25\text{--}30\text{meV}$, close to the maximum gap energy, Δ_0 . We summarize the temperature dependence of the energy at which we see a bosonic mode couple to the electronic states in the anti-nodal region in Fig. 2(d): the kink energies are at $\sim 40\text{meV}$ above T_c near the anti-nodal region and increase to $\sim 70\text{meV}$ below T_c . Because the band minimum is too close to E_F , the normal state $\sim 40\text{meV}$ kink cannot easily be seen below $\phi \sim 20^\circ$.

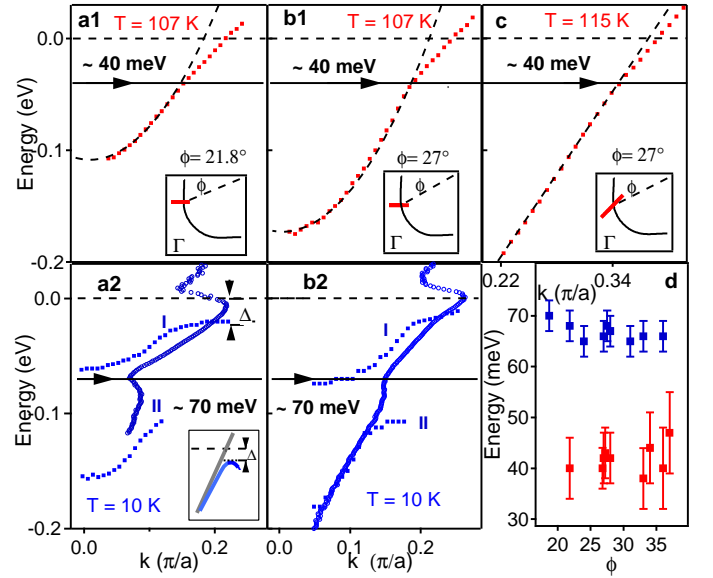


FIG. 2: EDC(a1, b1, c) derived dispersions in the normal state (107K and 115K). ϕ and the cut-direction are noted in the insets. The red dots are the data; the fit to the curve (dashes, black) below the 40meV line is a guide to the eye. a2) and b2) are MDC derived dispersions at the same location and direction as in a1) and b1), but in the superconducting state (15K). In a2) and b2) we also plot the peak(I) and hump positions(II) of the EDCs for comparison. The inset of a2) shows the expected behavior of a Bogoliubov type gap opening. The s-like shape below the gap energy is an artifact of how the MDC handles the back-bend of the Bogoliubov quasiparticle. d) kink positions as a function of ϕ in the anti-nodal region.

Now we turn to the momentum dependence shown in Fig. 3 that reveals two features defining the anisotropy

of the bosonic mode coupling. First, the coupling is extended in the Brillouin zone and has a similar energy scale throughout, near $\sim 65\text{-}70\text{meV}$. Second, the signatures of coupling increase significantly toward $(\pi, 0)$ or smaller ϕ . The clear minimum in spectral weight seen near 70meV in Fig. 3a1) and 3a2) indicates strong mixing of the electronic states with the bosonic mode where the two bare dispersions coincide in energy. In the same figure, we show how these distinctive features change as a function of doping. In the deeply overdoped sample ($T_c \sim 65\text{K}$ or $\delta \sim 22\%$), Fig. 3b, the kink energy moves to 40meV since Δ_0 ($\sim 10\text{-}15\text{meV}$) becomes much smaller. In the underdoped sample ($T_c \sim 85\text{K}$), the kink energy remains around 70meV since it has a similar gap as the optimally doped sample ($\Delta_0 \sim 35\text{-}40\text{meV}$). The signatures of coupling remain strong throughout, although they do noticeably increase from the overdoped to underdoped sample when comparing data taken at the same ϕ .

The above described experimental observations severely constrain the applicability of the spin resonance mode: 1.) We observe the 40meV boson in the normal state at optimal doping while the 41meV spin resonance mode exists only below T_c [17, 18] 2.) The kink is sharp in the superconducting state of a deeply over-doped Bi2212 sample (Fig. 3b, consistent with data of [7]) where no spin resonance mode has been reported, or is expected to exist since the spin fluctuation decreases strongly with doping. 3.) The kink seen in under-doped Bi2212 (Fig. 3c) is just as sharp as in the optimally doped case, while the neutron resonance peak is much broader [17, 18]. 4) Since the mode's spectral weight is only 2% [9], it may only cause a strong enough kink effect by highly concentrating in k -space [10]. Our data argues against this point as the bosonic renormalization effects exist in an extended k -space range.

We now propose an alternative interpretation for the anti-nodal renormalization effect as due to a coupling of the electronic states with the near 40meV B_{1g} phonon involving the out-of-plane motion of the in-plane oxygen [12]. Neutron scattering experiments show that this mode exhibits a clear softening across T_c only for $q < 0.5 \pi/a$ [12]. As depicted by the red arrows in Fig. 4a), this is consistent with a phonon coupling primarily states near the anti-node that can be connected with small q . A more complete picture, which we reserve for future discussion, would need to consider the 70meV half-breathing phonon shown to couple to the nodal states [2] and known to soften with doping by large q [19].

The question now is whether the assignment to the B_{1g} phonon can explain the coupling anisotropy and temperature dependence. We address the momentum dependence with a re-formulation of a previous theory [20]. The B_{1g} phonon preferentially couples to k points in the anti-nodal region of the BZ [13, 21]. Fig. 4a) and Fig. 4b) show the magnitude squared of the electron-phonon coupling vertex, $g^2(k, k')$, as a function of both the initial

momentum of the electron, k , and the phonon momentum, q , connecting k to $k' = k + q$ along the Fermi surface. An electron initially at the anti-node (k_{AN}), Fig. 4a), couples preferentially to other states in the anti-nodal region and especially favors $q \sim 2k_f$ scattering. An electron initially at the node (k_N), Fig. 4b), couples preferentially to states midway between the node and the anti-node. A comparison of Fig. 4a) and 4b) further reveals that $g^2(k, k')$ decreases substantially for an electron initially at the node. This momentum dependence in the electron-phonon coupling suggests that the signatures of strongest coupling should occur in cuts towards the anti-node, and parallel to the $(\pi, 0)$ - (π, π) line, as observed in the data. The strong momentum dependence also explains why the coupling constant inferred by ARPES measurements can be so different from the LDA value ($\lambda \sim 0.3$ for which the buckling mode dominates [22]) which represents an average of both k over the Brillouin zone and q over the momentum transfer. ARPES measurements correspond to a $\lambda \sim 2.8$ at the zone axes, but to an averaged $\lambda \sim 0.2$ and an even smaller value of the Raman λ that represents $q=0$. Within the context of this calculation, which relies on the framework of band theory, a quantitative comparison with the electron-phonon vertex derived from fitting Raman experiments [21] cannot be made. In order to do so, one has to consider vertex corrections which will affect the Raman and ARPES-derived coupling differently [23]. We leave these many body effects for future work.

Finally, we turn to the temperature dependence. Similar to ARPES data on Bi2212 reported here, tunneling data from a classical superconductor such as Pb shows wiggles due to electron-phonon coupling in the superconducting state, while they are hardly detectable in the normal state [24]. Motivated by the case of Pb, and other strongly-coupled conventional superconductors, we have solved the Eliashberg equations using a one-step iteration procedure as described in Sandvik et al. [11]. The self energy includes an electron-phonon coupling of the Bi2212 electronic structure described by a tight binding model fit to the measured dispersion and a d-wave gap in the superconducting state to the 40meV B_{1g} phonon with the $g^2(k, k')$ vertex shown in Fig. 4. Line cuts of the calculation close to the anti-node are compared with image plots of the data in Fig. 1. The calculations show that the dramatic increase of the effective coupling in the superconducting state can be attributed to the density of states enhancement due to the opening of the superconducting gap. The substantially higher temperature ($\sim 100\text{K}$) in the normal state also serves to broaden the phonon feature so that the dispersion exhibits, at most, a "kink" effect rather than a break up into two bands. The complete analysis of this calculation will be presented in a subsequent paper [20].

In summary, based on extensive temperature, momentum, and doping dependent data and a theoretical calculation, we propose a new interpretation of the bosonic

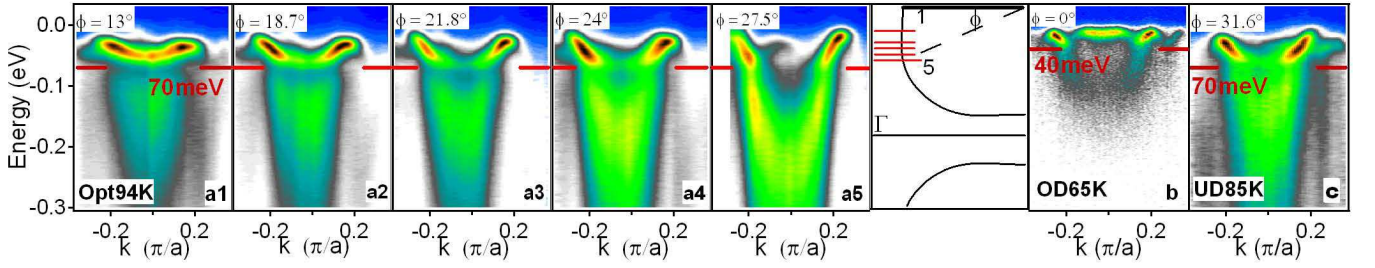


FIG. 3: The image plots in a1-a5 are cuts taken parallel to $(0,\pi)-(\pi,\pi)$ at the locations indicated in the zone at 15K for an optimally doped sample (94K). b) and c) are spectra taken parallel to $(0,\pi)-(\pi,\pi)$ at the k -space locations indicated for over-doped (65K) and under-doped samples (85K) respectively.

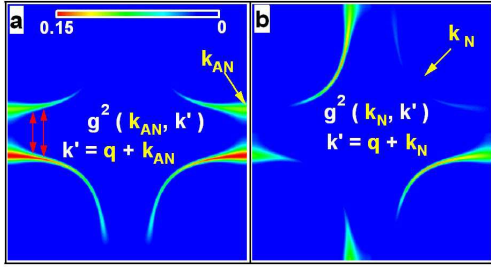


FIG. 4: a) and b) image plots of $g^2(k, k')$ for the B_{1g} bond-buckling phonon on the Fermi Surface of Bi2212. $k' = k + q$, where k is the initial momentum of the electron and q is the momentum of the phonon. a) represents $g^2(k_{AN}, k')$ for an electron initially at the anti-node. We draw red arrows indicating the dominant $q \sim 2k_F \sim 0.5\pi/a$ scattering; b) represents $g^2(k_N, k')$ for an electron initially at the node

mode renormalization seen in ARPES as electronic coupling to the B_{1g} bond-buckling phonon. The dominance of the renormalization near the anti-node indicates its potential importance to the pairing mechanism, which is consistent with some theory [22, 25, 26, 27] but remains to be investigated.

-
- [1] P.V. Bogdanov *et al.*, Phys. Rev. Lett. **85**, 2581 (2000)
 - [2] A. Lanzara *et al.*, Nature **412**, 510 (2001)
 - [3] X.J. Zhou *et al.* Nature **423**, 398 (2003)
 - [4] P.D. Johnson *et al.*, Phys. Rev. Lett. **87**, 177007 (2001)
 - [5] A. Kaminski *et al.*, Phys. Rev. Lett. **86**, 1070 (2001)
 - [6] T.K. Kim *et al.*, Phys. Rev. Lett. **91**, 167002 (2003)
 - [7] A.D. Gromko *et al.*, Phys. Rev. B, **68**, 174520 (2003)
 - [8] T. Sato *et al.*, Phys. Rev. Lett. **91**, 157003 (2003)
 - [9] H.-Y. Kee, S.A. Kivelson, G. Aeppli, Phys. Rev. Lett. **88**, 257002 (2002)
 - [10] A. Ababnov *et al.*, Phys. Rev. Lett. **89**, 177002 (2002)
 - [11] A. W. Sandvik, D. J. Scalapino, N.E. Bickers cond-mat/0309171, xxx.lanl.gov, (2003)

- [12] D. Reznik *et al.*, Phys. Rev. Lett. **75**, 2396 (1995)
- [13] T.P. Devereaux *et al.*, Phys. Rev. B **59**, 14618 (1999)
- [14] S. Engelsberg and J.R. Schrieffer Phys. Rev. **131**, 993 (1963)
- [15] S. LaShell, E. Jensen, T. Balasubramanian Phys. Rev. B **61**, 2371 (2000)
- [16] J.J. Tu *et al.* Phys. Rev. B **66**, 144514 (2002) These authors report a mode but they do not identify its origin; the main thesis is to support the spin resonance.
- [17] H.F. Fong Phys. Rev. Lett. **75**, 316 (1995)
- [18] P. Dai *et al.*, Phys. Rev. B **63**, 054525 (2001)
- [19] S.L. Chaplot *et al.*, Phys. Rev. B **52**, 7230 (1995); O.K. Andersen *et al.*, Phys. Rev. B **49**, 4145-4157 (1994).
- [20] T.P. Devereaux *et al.*, xxx.lanl.gov, cond-mat/0403766 (2004)
- [21] M. Opel *et al.*, Phys. Rev. B **60**, 9836 (1999)
- [22] O. Jepsen *et al.*, J. Phys. Chem. Solids **59**, 1718 (1998); O.K. Andersen *et al.*, J. of Low Temp. Phys. **105**, 285 (1996).
- [23] O. Rosch and O. Gunnarsson, private communication
- [24] D.J. Scalapino, J.R. Schrieffer, J.W. Wilkins, Phys. Rev. **148**, 263 (1966)
- [25] K.A. Muller, Proceedings of the 10th Anniversary HTS Workshop, March 12-16., Edited by B. Batlogg *et al.*, (World Scientific, Houston, 1996)
- [26] D.J. Scalapino, J. Phys. Chem. Solids **56**, 1669 (1995)
- [27] A. Nazarenko and E. Dagotto, Phys. Rev. B **53**, R2987 (1996)
- [28] We thank R.B. Laughlin, K.A. Muller, H. Keller, O. Gunnarsson, D.H. Lee, D.J. Scalapino, A. Lanzara, A. Fujimori, S. Tajima, S. Kivelson, and D.I. Santiago for stimulating discussions. ZXS thanks the Physics Institute of the University of Zurich and especially Prof. Jurg Osterwalder for the hospitality. T. Cuk, F. Baumberger, and TPD, acknowledge funding from the National Science Foundation, the Swiss National Science Foundation, and the NSERC, PREA, and Alexander von Humboldt Foundation, respectively. ARPES experiments were performed at the Stanford Synchrotron Radiation Laboratory (SSRL) with DOE contract DE-AC03-76SF00515. The Stanford work was also supported by NSF grant DMR-0304981 and ONR grant N00014-01-1-0048.